ACS OMEGA

http://pubs.acs.org/journal/acsodf

Article

High-Field One-Dimensional and Two-Dimensional ^{27}Al Magic-Angle Spinning Nuclear Magnetic Resonance Study of θ-, δ-, and γ-Al_2O_3 Dominated Aluminum Oxides: Toward Understanding the Al Sites in γ-Al_2O_3

Suochang Xu, Nicholas R. Jaegers, Wenda Hu, Ja Hun Kwak, Xinhe Bao, Junming Sun, Yong Wang,* and Jian Zhi Hu*

Cite This: *ACS Omega* 2021, 6, 4090−4099

Read Online

ACCESS | Metrics & More | Article Recommendations | Supporting Information

ABSTRACT: Herein, a detailed analysis was carried out using high-field (19.9 T) ^{27}Al magic-angle spinning (MAS) nuclear magnetic resonance (NMR) on three specially prepared aluminum oxide samples where the γ-, δ-, and θ-Al_2O_3 phases are dominantly expressed through careful control of the synthesis conditions. Specifically, two-dimensional (2D) multiquantum (MQ) MAS ^{27}Al was used to obtain high spectral resolution, which provided a guide for analyzing quantitative 1D ^{27}Al NMR spectra. Six aluminum sites were resolved in the 2D MQ MAS NMR spectra, and seven aluminum sites were required to fit the 1D spectra. A set of octahedral and tetrahedral peaks with well-defined quadrupolar line shapes was observed in the θ-phase dominant sample and was unambiguously assigned to the θ-Al_2O_3 phase. The distinct line shapes related to the θ-Al_2O_3 phase provided an opportunity for effectively deconvoluting the more complex spectrum obtained from the δ-Al_2O_3 dominant sample, allowing the peaks/quadrupolar parameters related to the δ-Al_2O_3 phase to be extracted. The results show that the δ-Al_2O_3 phase contains three distinct Al_O sites and three distinct Al_T sites. This detailed Al site structural information offers a powerful way of analyzing the most complex γ-Al_2O_3 spectrum. It is found that the γ-Al_2O_3 phase consists of Al sites with local structures similar to those found in the δ-Al_2O_3 and θ-Al_2O_3 phases albeit with less ordering. Spin−lattice relaxation time measurement further confirms the disordering of the lattice. Collectively, this study uniquely assigns ^{27}Al features in transition aluminas, offering a simplified method to quantify complex mixtures of aluminum sites in transition alumina samples.

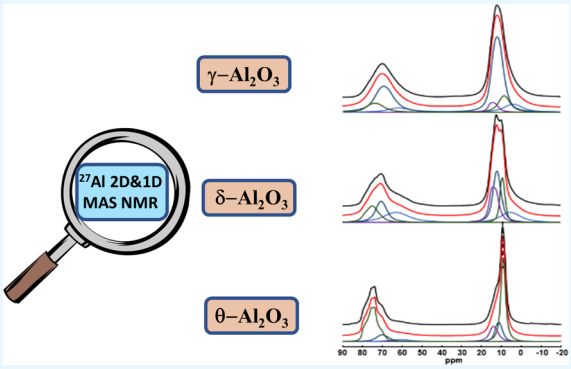

INTRODUCTION

Transition aluminum oxides comprise an important class of materials broadly used across industries as catalysts, catalyst supports, adsorbents, hard protective coatings, abrasives, and membranes.[1−7] They impart such wide utilization due to their attractive structural, surface, and dielectric properties.[8] The structural stability, including the ability to maintain high surface area at elevated temperatures, is a key consideration solidifying the relevance of these materials in catalytic applications. Among the phases, γ-Al_2O_3 is the most prominent polymorph in catalytic applications due to its high surface area and structural stability up to the temperatures of 700−800 °C. However, after prolonged exposure to temperatures exceeding 800 °C, γ-Al_2O_3 transforms into δ-Al_2O_3 and θ-Al_2O_3 (∼1000 °C) polymorphs. At even further extended times and temperatures in excess of 1200 °C, the alumina finally converts to α-Al_2O_3, the most thermodynamically stable Al_2O_3 structure.[9,10] A key consequence associated with these phase transformations is a dramatic reduction in surface area, which deteriorates catalytic properties. For this reason, considerable experimental and theoretical investigations have been devoted in the past to understand the structural properties of γ-Al_2O_3 and the thermodynamic and kinetic factors that dictate its stability. It is now becoming well-understood that stabilization of transition Al_2O_3 with respect to α-Al_2O_3 can be achieved for very small crystallites as a consequence of low surface energy.[11] Extensive work has also focused on how to enhance the structural stability of the particle and understand the underlying mechanism of sintering. For example, it is found that by doping BaO or La_2O_3 onto the surface, the thermal stability of γ-Al_2O_3 is dramatically improved.[12,13]

Received: December 18, 2020
Accepted: January 14, 2021
Published: January 25, 2021

Although significant advances have been made in the field of transition Al_2O_3,[14,15] the nature of the phase transformation at the early stages, γ-Al_2O_3 transforming to δ-Al_2O_3 and subsequently to θ-Al_2O_3, is the least understood. It should be noted that phase transitions that bypass δ-Al_2O_3 have also been observed.[16] A key reason for this lack of understanding is the ambiguity in the structure of γ-Al_2O_3,[17−23] which accommodates substantial defects to the microstructure, as well as the complex crystallographic structure of δ-Al_2O_3, which can also accommodate significant disorder.[24−27] Such δ-Al_2O_3 has been described as a complex intergrowth of two variants δ_1 and δ_2;[25,27] however, the nature of such a δ-Al_2O_3 phase has been shown to be more complex. δ-Al_2O_3 is actually described as adopting two intergrowth structures that are differentiated by their variant selection and intergrowth direction, $\delta_{1,2}$ and $\delta_{2,3,4}$.[26] To compound this issue, the coexistence of different transition Al_2O_3 phases in the same sample during heating has made it very challenging to probe the fine and irregular structures by traditional analytical techniques. One novel method to address this issue is to employ a recursive stacking methodology, accounting for the intergrowth modes of δ-Al_2O_3 and θ-Al_2O_3.[28] This is complicated by the amorphous domains, which are generated at the interfaces of ordered regions in the alumina crystals and impart disorder that cannot yet be fully accounted for with such a technique. Traditional XRD techniques, for example, require long-range order to understand the structure of alumina, which is complicated by the presence of a significant quantity of disordered regions. If crystals are free of strain and faulting, then peak broadening is only ascribed to domain size, which can be calculated by the Scherrer equation.[29] However, if the structure is amorphous or the nanoparticle size is smaller than 2 nm, then low signal to noise ratios and decreased detector sensitivity make the detection difficult and uncertain. The state-of-art XRD limitation is 1.2 nm on Au particles supported on carbon by using high sensitivity silicon slit detectors.[30] Chauhan et al. published a review on the XRD technique and its applications, demonstrating that a periodic array with long-range order is needed for diffraction to occur while the amorphous materials without long-range order do not display any significant peak in the diffraction pattern.[31]

Solid-state ^{27}Al nuclear magnetic resonance (NMR) is a powerful technique for investigating the structural transformations and surface structure of alumina.[32−37] In particular, distinct NMR peaks are obtained for the tetra-, penta-, and octahedral aluminum sites present in various transition Al_2O_3 phases, as Chandran et al. recently reviewed.[38] Such an identification of the type of alumina present extends to the amorphous regions where other techniques, in particular for XRD, would fail due to the lack of long-range order since NMR is impacted primarily by the local environment. ^{27}Al is a quadrupolar nucleus with a spin quantum $I = 5/2$ and is thus subject to quadrupolar line broadening. Because such line broadening is inversely proportional to the external magnetic field strength,[39] the resolution in magic-angle spinning (MAS) ^{27}Al spectra of γ-Al_2O_3 obtained at low to medium magnetic fields is relatively poor, hindering clear separation of the peak corresponding to the penta-coordinated aluminum ions from those corresponding to the tetrahedral and octahedral aluminum. As such, the use of MAS NMR to study the relationship of the transition Al_2O_3 surface structure to its material and catalytic properties has been correspondingly limited. Only recently was high magnetic field NMR used to study the phase transition process of γ-Al_2O_3, with much improved spectral resolution over low magnetic fields for characterizing different alumina phases during the calcination.[40] A higher magnetic field is of great importance to provide better resolution for Al-containing compounds, such as higher resolution in an HBEA zeolite study[41] and identification of penta-coordinated Al sites in γ-Al_2O_3.[42] Our prior studies, conducted at a high field of 21.1 T, were the first to highlight the high-quality spectra of γ-Al_2O_3 with clearly separated tetra-, penta-, and octahedral aluminum sites.[13,42]

Multiple-quantum (MQ) MAS 2D NMR techniques[43,44] offer enhanced spectral resolution along the second dimension of a 2D NMR spectrum. The application of this technique to clearly resolve and assign spectral features to aluminum sites in tetra-, penta-, and octahedral coordinations was previously demonstrated.[45−47] Despite its remarkably rapid acceptance as an important technique for structural studies of a broad range of solid materials, especially microporous solids, glasses, and novel metal oxides, the MQ MAS experiment has aspects that still require further development. MQ MAS is, in general, not quantitative as there is no established method to allow uniform excitation and detection of multiple-quantum coherence that is independent of the magnitude of the quadrupolar coupling. In contrast, the very sensitive 1D MAS spectra (obtained at high fields and high spinning rates) are intrinsically quantitative, given appropriate experimental conditions. In these cases, the second-order line broadening is not eliminated but rather progressively narrowed at increasing magnetic fields.

In this work, three specially synthesized transition Al_2O_3 samples where the γ-, δ-, or θ-Al_2O_3 dominates are studied using a combined 1D ^{27}Al MAS NMR and 2D MQ MAS experimental approach and coupled with spin−lattice relaxation techniques at a high field (19.9 T). This work assigns the observed spectral features to Al sites, which are present in the θ-Al_2O_3 and δ-Al_2O_3 phases, including the γ-Al_2O_3. The NMR parameters of different aluminum sites are extracted from the 2D MQ MAS NMR spectra and used to fit the signals obtained from the quantitative 1D MAS spectra, giving rise to quantitative distributions and spin−lattice relaxation times for different transition Al_2O_3 sites. To our knowledge, this is the first attempt to understand the aluminate sites in γ-Al_2O_3, where the advantages of the distinct line shapes from specially synthesized δ- and θ-Al_2O_3 dominated phases are utilized to gain deep insights into the aluminate site structures of the very complex γ-Al_2O_3 sample. Note that NMR is a powerful local structural probe where the local site structures can be probed, in particular the amorphous phase that can be especially emphasized by using a short recycle delay time due to its much shorter spin−lattice relaxation time compared to the crystalline phases, offering distinct advantages over the commonly used XRD technique.

RESULTS AND DISCUSSION

The previously reported XRD patterns of the prepared alumina samples show that multiple phases of alumina exist in each of the samples.[25] The XRD pattern of the 800 °C calcined sample, γ-Al_2O_3 (Figure S1a), primarily consists of diffraction peaks consistent with γ-Al_2O_3 but are accompanied by a peak at $2\theta = 46.4°$ indicative of δ-Al_2O_3, albeit visible with low peak intensity. The 1000 °C calcined sample, δ-Al_2O_3 (Figure S1b), exhibits features consistent with δ-, θ-, and γ-Al_2O_3 phases, where the sharp peaks at 2θ values of 46.4 and 32.6° are characteristic peaks for δ-Al_2O_3 crystals. Simulations of the

https://dx.doi.org/10.1021/acsomega.0c06163
ACS Omega 2021, 6, 4090−4099

overall XRD pattern without considering recursive stacking revealed that about 72% of the samples in crystallite forms in this sample are from the δ-Al_2O_3 phase (Table 1).[25,27] Figure S1c reflects a higher abundance of θ-Al_2O_3 (69%) as is obvious by the group of sharp peaks at 2θ values of about 31.8, 32.6, 44.8, 47.5, 51, 60, 62.5, 64, 66, and 67°. These three samples are labeled γ-, δ-, and θ-Al_2O_3, respectively, to emphasize the dominant phase present in each sample. These samples correspond to crystallite sizes of 7 ± 2, 15 ± 1, and 23 ± 4 nm, respectively. The quantitative estimations of the fractions of alumina polymorphs in the nanoparticles using XRD are often difficult to generalize for metastable alumina phases that are not well-distinguished from the XRD patterns and characterized by complex intergrowths of variants. Furthermore, standard XRD pattern acquisition requires periodicity of the lattice to obtain a diffractogram, a requirement not met under highly amorphous conditions. For XRD to generate a peak, a particle with periodic lattice structure and dimensions greater than 2 nm is required. Complementarily, NMR is sensitive to local structural changes and does not require such a long-range order. Herein, we attempt to deconvolute and quantify the types of sites present in each prepared sample. It should be emphasized that different alumina phases are concepts of XRD analysis only, while ^{27}Al NMR gives the aluminum site distributions in the octahedral, tetrahedral, and penta-Al site regions. Rigorous and quantitative correlation between NMR and XRD is impossible given the fact that surface aluminum sites such as penta-coordinated aluminum sites are not detected. Though XRD gives a signal that is a function of all atoms in the sample (including disordered and amorphous structures), the disordered and amorphous regions are usually disregarded, and XRD analysis typically looks at the ordered fraction of the domain with dimensions of greater than 2 nm. Thus, the current NMR analysis complements XRD studies and offers new insights into the aluminum site distribution.

Table 1. XRD Results for the Prepared Al_2O_3 Samples

sample	XRD determined phase ratio	crystallite size (nm)
γ-Al_2O_3	100% γ-Al_2O_3	7 ± 2
δ-Al_2O_3	52% δ_1-Al_2O_3	15 ± 1
	20% δ_2-Al_2O_3	
	28% θ-Al_2O_3	
θ-Al_2O_3	31% δ_1-Al_2O_3	23 ± 4
	69% θ-Al_2O_3	
	0.6% α-Al_2O_3	

Figure 1 presents the high-resolution solid-state ^{27}Al MAS NMR spectra of these alumina samples. Figure 1a, obtained from the γ-Al_2O_3 sample, is similar to previously reported spectra.[13,42] The spectrum consists of three major peaks centered at 12.8, 35, and 70.6 ppm due to Al^{3+} cations in octa- (Al_O), penta- (Al_P), and tetrahedral (Al_T) coordination, respectively. It should be emphasized again that γ-Al_2O_3 is purely an XRD identification based on the fairly broad XRD diffraction peaks in Figure S1a (i.e., lacking fine diffraction peaks). It is generally accepted that the structures in γ-Al_2O_3 are very complex and are also poorly understood in the literature. In this work, we will be able to provide new insights into the aluminum site distributions in the γ-Al_2O_3 sample by taking advantage of the specially synthesized δ-Al_2O_3 and θ-Al_2O_3 phase dominated samples. In the δ-Al_2O_3 sample

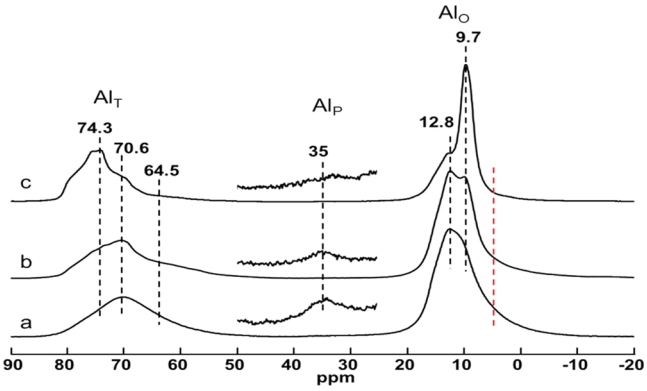

Figure 1. 1D ^{27}Al MAS NMR spectra with a recovery time of 80 s for the three transition Al_2O_3 samples (a) γ-Al_2O_3, (b) δ-Al_2O_3, and (c) θ-Al_2O_3 (inserted are ×10).

(Figure 1b), two distinct Al_O features emerge, centered at ∼10.2 and ∼12.8 ppm. Careful examination of the spectral features in Figure 1a reveals that these two Al_O features are also present in the γ-Al_2O_3 sample albeit the peak linewidth is broader. The Al_T shoulder peak feature at 64.5 ppm, a break point of a quadrupolar line shape as will be made clear later, is clearly visible in both Figure 1a and Figure 1b. In the θ-Al_2O_3 spectrum (Figure 1c), the octahedral Al_O peaks are dominated by a strong resonance located at about 9.7 ppm. Further, the intensity of the shoulder at 64.5 ppm is weaker than that of δ-Al_2O_3 but still visible. An additional peak with a well-defined quadrupolar second-order line shape with a dominant break point located at about 74.3 ppm stands out in θ-Al_2O_3. According to the XRD results, this sample exhibits a dominating θ-Al_2O_3 phase (69%). As such, the feature peaks present at 9.7 and 74.3 ppm are safely assigned to the octa- and tetrahedral aluminum sites, which are associated with the θ-Al_2O_3 phase. This is consistent with previous assignments by O'Dell et al., where the ^{27}Al MAS NMR spectrum was acquired at a lower magnetic field of 14.1 T.[34] Given the assignments of the Al_O and Al_T peaks for the θ-Al_2O_3 phase in Figure 1c, the sets of the peak features at 10.2 ppm (Al_O) and ∼74 ppm (Al_T) in the δ-Al_2O_3 dominated sample (Figure 1b) can be assigned to the Al_O and Al_T sites associated with the θ-Al_2O_3 structure. Since Figure 1b contains 72% of the δ-phase based on XRD, the major spectral features must be associated with the δ-phase. Thus, the dominant Al_O peak centered at ∼12.8 ppm and the dominant Al_T peak feature located at about 70.6 ppm (a break point of quadrupolar line shape) in Figure 1b are attributed to the spectral features associated with δ-Al_2O_3. With a close examination of the peak line shapes in both the octahedral and the tetrahedral spectral ranges in Figure 1, it becomes apparent that γ-Al_2O_3 consists of all spectral features associated with the δ-Al_2O_3 and θ-Al_2O_3 samples albeit the corresponding spectral features are broadened and the distribution of the Al sites is different. The increased line broadening is a direct consequence of the considerably increased disordering of the polycrystal structures, reflected by the significantly reduced crystallite sizes (7.5 nm for γ-, 15 nm for δ-, and 23 nm for δ-Al_2O_3) from XRD measurement.

The fact that γ-Al_2O_3 contains aluminum sites (Al_O and Al_T) similar to δ-Al_2O_3 and θ-Al_2O_3 is quite reasonable since the peak position in an NMR spectrum is only sensitive to the local electronic structure surrounding the observed Al site (i.e., up to about 1 nm), and δ-Al_2O_3 was previously described by a

https://dx.doi.org/10.1021/acsomega.0c06163
ACS Omega 2021, 6, 4090−4099

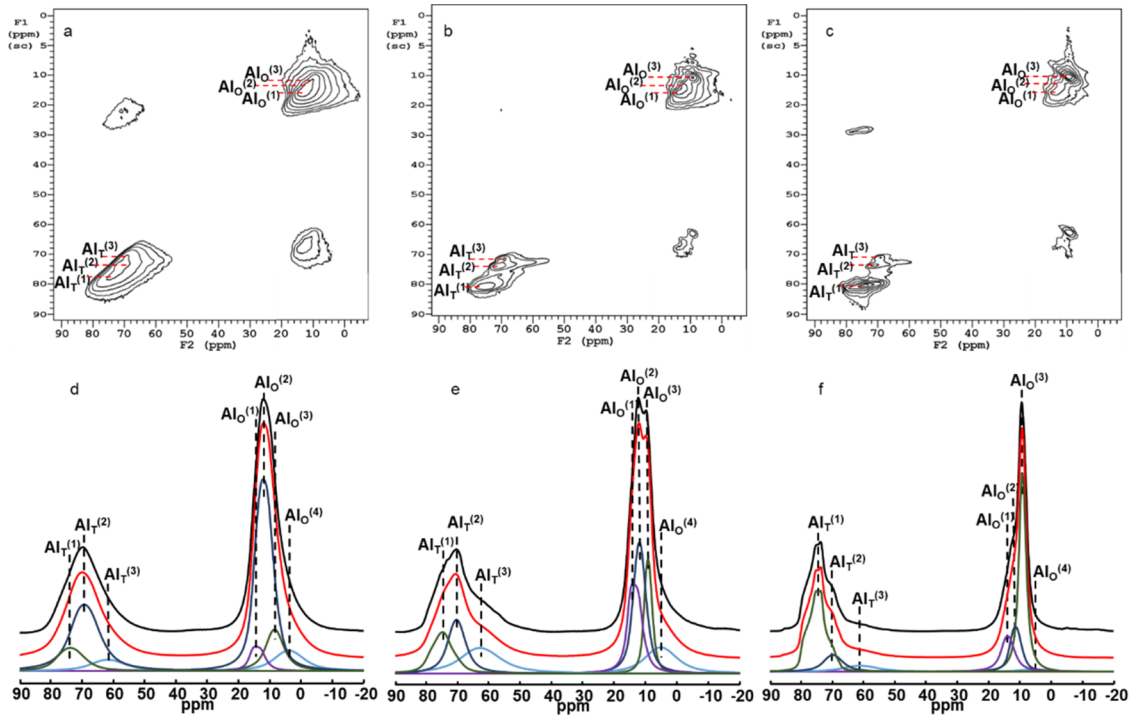

Figure 2. 2D ^{27}Al 3Q MAS NMR spectra of (a) γ-Al_2O_3, (b) δ-Al_2O_3, and (c) θ-Al_2O_3 with a 5 s recycle delay; (d–f) corresponding 1D MAS NMR spectrum (top) of them and their simulated spectrum (bottom) using the Q mas $^1/_2$ model in DMFIT (the red line in the middle is the sum of the individual fitting lines). Pentahedral sites are not simulated due to their low intensity.

Table 2. Spectroscopic Parameters Including Isotropic Chemical Shifts (δ_{iso}), Quadruple Coupling Constants (C_Q), and Asymmetry Parameters (η) of Al Peaks and Their Relative Integrated Intensities in the Three Samples

sample	peak (Al site)	δ_{iso} (±1 ppm)	C_Q (±0.1 MHz)	η (±0.1)	intensity (%)	Al site structure assignments	alumina phase %
γ-Al_2O_3	$Al_O^{(1)}$	16.9	4.9	0.0	3.6	local structures similar to δ	
	$Al_O^{(2)}$	15.7	5.5	0.4	42.8	local structures similar to δ	
	$Al_O^{(3)}$	11.0	4.4	0.5	9.2	local structures similar to θ	100% γ-Al_2O_3
	$Al_O^{(4)}$	8.6	6.0	0.6	7.9	disordered, local structures similar to δ	
	$Al_T^{(1)}$	78.8	6.4	0.5	8.4	local structures similar to θ	
	$Al_T^{(2)}$	73.9	6.1	0.5	22.4	local structures similar to δ	
	$Al_T^{(3)}$	67.5	6.6	0.6	5.7	disordered, local structures similar to δ	
δ-Al_2O_3	$Al_O^{(1)}$	16.3	4.8	0.0	17.0	δ	
	$Al_O^{(2)}$	14.5	4.3	0.6	22.3	δ	
	$Al_O^{(3)}$	10.8	3.5	0.5	12.0	θ	77.1% δ
	$Al_O^{(4)}$	9.8	5.9	0.6	11.3	disordered δ	22.9% θ
	$Al_T^{(1)}$	80.0	6.0	0.7	10.9	θ	
	$Al_T^{(2)}$	73.2	4.6	0.6	12.9	δ	
	$Al_T^{(3)}$	68.3	6.6	0.4	13.6	disordered δ	
θ-Al_2O_3	$Al_O^{(1)}$	15.8	4.0	0.0	11.2	δ	
	$Al_O^{(2)}$	13.2	2.9	0.3	11.5	δ	
	$Al_O^{(3)}$	10.2	3.5	0.5	33.8	θ	37.3% δ
	$Al_O^{(4)}$	9.7	5.9	0.6	1.4	disordered δ	62.7% θ
	$Al_T^{(1)}$	80.3	6.2	0.7	28.9	θ	
	$Al_T^{(2)}$	73.0	4.9	0.5	7.3	δ	
	$Al_T^{(3)}$	66.7	6.6	0.4	4.5	disordered δ	

superstructure of γ-Al_2O_3 with the *c*-axis tripled because of the increased ordering of cationic vacancies on octahedral sites.[10,48] A similar local environment around Al^{3+} will result in the same peak position associated with these two Al_2O_3 phases. It is also reasonable considering the diverse sites identified for δ-Al_2O_3, which is composed of four variants that likely broaden the effective spectral features for the phase and contribute to a signal composed of several species with similar environments. Based on TEM studies, δ_1-Al_2O_3 alone presents 10 unique octahedral sites and 6 unique tetrahedral sites, highlighting the potential for further ambiguity in peak position. Among all variants, there exist 57 unique sites in delta, in addition to the disordered transition zones (δ_1: 10, 6; δ_2: 10, 6; δ_3: 6, 3; and δ_4: 10, 6 for octahedral and tetrahedral, respectively).

https://dx.doi.org/10.1021/acsomega.0c06163
ACS Omega 2021, 6, 4090−4099

It becomes apparent that the 12.8 ppm peak in Figure 1b is narrower than the corresponding 12.8 ppm peak in Figure 1a primarily due to the increased ordering in the δ-Al_2O_3 phase compared with γ-Al_2O_3. It is known from the XRD studies summarized in Table 1 that the crystallite sizes for the samples increase with thermal treatment, showing a higher degree of order at samples expressing higher contents of later phases. Further, the intensity of the Al_P sites was previously proposed as a reflection of the amount of disorder in aluminum samples[49] since no Al_P sites exist in the idealized crystalline Al_2O_3 phases. From γ- and δ- to θ-Al_2O_3 dominant samples, the intensity of Al_P sites decreases, showing that the structure is getting more and more ordered, consistent with the crystal size evolution. Compared with γ-Al_2O_3 and δ-Al_2O_3, the intensity of the tail on the low Al_O ppm side (reflected by the red dashed line) in θ-Al_2O_3 is significantly decreased. The more symmetric line shape in θ-Al_2O_3 indicates that the structure is more ordered in this sample. The ^{27}Al experiments conducted at a high magnetic field thus offer insights into the material structure changes that occur across thermal treatments, indicated by changes to the resonance feature evolution.

The results of ^{27}Al 3Q MAS NMR provide new insights into the nature of the electronic environment around Al^{3+} cations in these nanostructured transition aluminas. Examples of sliced spectra from 3Q MAS NMR on γ-Al_2O_3 are also reported previously.[3] As can be seen in Figure 2b,c, 2D 3Q MAS NMR spectra of these two specially prepared nanostructure transition aluminas show significantly enhanced spectral resolution. This allows at least three different aluminum sites to be unambiguously detected in both the octahedral and tetrahedral coordinated environments in these two samples. In the octahedral region, on the $Al_O^{(1)}$ site, which was not well-resolved in the 1D MAS spectra, a feature is distinguished in the 2D experiment. The absence of Al_P sites in all of the 2D experiments shown here is due to their low abundance and an insufficient quantity of the accumulation number in data acquisition. This is no surprise as it is well-known that 2D 3Q MAS experiments offer the highest possible spectral resolution but at the expense of sensitivity and quantitative information when compared with 1D MAS experiments. Despite the lower sensitivity and the loss of quantification compared with quantitative 1D NMR, the isotropic chemical shifts (δ_{iso}), quadruple coupling constants (C_Q), and asymmetry parameters (η) can be obtained from 3Q MAS NMR spectra (Table 2), offering unique information for characterizing the different Al sites. These parameters were obtained by fitting 1D spectra using the DMFIT program on sliced spectra that were extracted parallel to the F2 (acquisition) dimension and at various F1 (isotropic) dimensions. These same parameters were then used to deconvolute the 1D spectrum (Figure 2d–f) as a strategy for obtaining quantitative information of different aluminum sites (Table 2). It is necessary to use an additional octahedral resonance peak, $Al_O^{(4)}$, in all three samples in order to fit the spectrum.

Based on the results from 1D and 2D NMR, it is apparent that all three samples are complex mixtures of different alumina phases, in agreement with the XRD results discussed earlier. However, rigorous assignment of each individual peak to an XRD-identified phase is difficult due to the fact that XRD is a method based on long-range order, while NMR is a local structure-sensitive structure probe with a detection limit not reliant on periodicity. Thus, only those ^{27}Al peaks associated with long-range order can be safely associated with an XRD-identified phase, while the peaks associated with more disordered environments, in particular the amorphous phase, can only be assigned to specific new Al sites. Herein, we will only attempt to establish a rough correlation between NMR and XRD results. Based on 1D and 2D NMR results and previously reported NMR parameters of different aluminum species/sites, assignments can be made for the individual simulated peaks, which are summarized in Table 2. The $Al_O^{(1)}$ site has a chemical shift (16.9 ppm) near the chemical environment of the α-Al_2O_3 phase.[50] However, no α-Al_2O_3 phase was detected by XRD in the γ- and δ-Al_2O_3 samples (Figure S1a,b), and the temperature of treatment was too low for this stable phase to form to a significant extent.[17,24] In addition, the XRD-reported 0.6% for the α-Al_2O_3 phase in the θ-Al_2O_3 dominant sample would be too low to be observed by current ^{27}Al 1D and 2D NMR. This Al^{3+} cation exhibits an integrated intensity, which is modulated from 3.6 to 17% and then to 11.2%. Such a decrease would be unexpected for α-Al_2O_3 phase formation given the better crystallinity of the θ-Al_2O_3 sample overall and the higher propensity to generate α-Al_2O_3 under such conditions. Since the abundance is highest in the samples that preferentially express the δ-phase dominant sample, this signal is assigned to octahedral aluminum sites in Al_2O_3, which are associated with one of the many δ-phase structures that have a local electronic structure (within 1 nm) similar to that of the α-Al_2O_3 octahedral site given the similarity of the experimentally observed chemical shift value of 16.9 ppm to that of α-Al_2O_3.

Based on the presence of the $Al_O^{(2)}$ and $Al_T^{(2)}$ features across all samples with decreasing abundance (42.8/22.4%, 22.3/13.0%, and 11.5/7.3% for $Al_O^{(2)}$ and $Al_T^{(2)}$, respectively), these sites are assigned to aluminum sites associated with the δ-Al_2O_3 phase for the δ-Al_2O_3 and θ-Al_2O_3 dominated samples (Figure 1b) since there are no γ-Al_2O_3 phases detected in these two samples. Then, the question arises on what the $Al_O^{(2)}$ and $Al_T^{(2)}$ features in the γ-Al_2O_3 sample belong to. The ratio of $Al_O^{(2)}/Al_T^{(2)}$ determined from the experimental data is 1.91, 1.72, and 1.57 for γ-Al_2O_3, δ-Al_2O_3, and θ-Al_2O_3 dominated samples, respectively. Based on XRD studies, it is commonly accepted that the oxygen lattice for γ- and δ-Al_2O_3 phases is the same; the difference is in the ordering of the Al atoms. It has been suggested that aluminum cation rearrangement occurs and that vacancies are distributed among octahedral (O_h) and tetrahedral (T_d) sites in γ-Al_2O_3 but ordered solely on octahedral sites in δ-Al_2O_3.[48,51,52] In general, defective spinel-like models are used to describe their structures, though departures from the spinel representation of the structure with the occupation of non-spinel sites have also been proposed.[17,19−23] In a spinel structure, the Al^{3+} distribution can vary between 62.5% O_h and 37.5% T_d (O_h/T_d = 1.66) when assuming that vacancies occupy exclusively O_h interstices[19] and 75% O_h and 25% T_d (O_h/T_d = 3) when vacancies are supposed to be exclusively located in T_d sites. Thus, the ratio of $Al_O^{(2)}/Al_T^{(2)}$ in the three samples to some extent agrees with the proposal that vacancies are distributed randomly in the γ-Al_2O_3 phase and ordered almost exclusively on O_h sites in the δ-Al_2O_3 and θ-Al_2O_3 phase dominant samples. Note that the ratios of $Al_O^{(2)}/Al_T^{(2)}$ in our δ- and θ-Al_2O_3 samples are close to that of ideal δ-Al_2O_3 (1.66). This explains why the amount of the γ-phase is not detected by XRD (Table 1). We can, however, note some differences by comparing the ratio of Al_O/Al_T for the two phases as well as the C_Q values of $Al_O^{(2)}$ and

https://dx.doi.org/10.1021/acsomega.0c06163
ACS Omega 2021, 6, 4090−4099

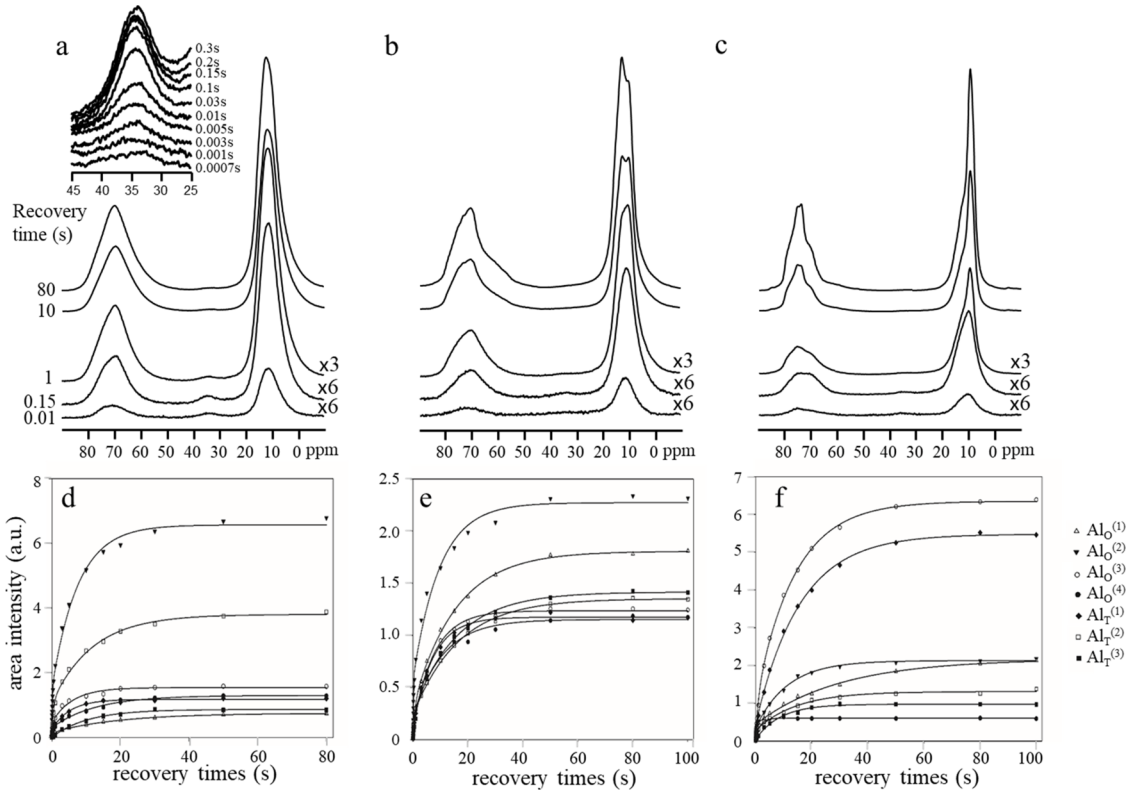

Figure 3. Spin−lattice relaxation NMR spectra. (a−c) ^{27}Al MAS NMR spectra of the prepared alumina samples as a function of several selected recovery times. (a) γ-Al_2O_3 (inserted pentahedral aluminum of γ-Al_2O_3, the accumulation number used is 3000), (b) δ-Al_2O_3, and (c) θ-Al_2O_3. (d−f) Integrated ^{27}Al MAS NMR spectral intensity of each site as a function of the saturation recovery time in (d) γ-Al_2O_3, (e) δ-Al_2O_3, and (f) θ-Al_2O_3.

$Al_T^{(2)}$ sites. C_Q in the δ- and θ-Al_2O_3 samples is smaller than that of γ-Al_2O_3 and low-field literature reports of 5.5 MHz,[36] indicating that the structures of $Al_O^{(2)}$ and $Al_T^{(2)}$ sites are more ordered (i.e., with a longer range of periodic structures) in the δ- and θ-Al_2O_3 samples, consistent with XRD results.

Two additional Al sites, $Al_O^{(4)}$ and $Al_T^{(3)}$, reflect relatively high C_Q values that are apparently associated with more disordered structures due to less symmetry of the electric structures around the corresponding Al sites. Compared to the $Al_O^{(4)}$ and $Al_T^{(3)}$ in the γ-Al_2O_3 dominated sample (7.9 and 5.7%, respectively), the intensities of the $Al_O^{(4)}$ and $Al_T^{(3)}$ sites increased in the δ-Al_2O_3 dominated sample to 11.3 and 13.6% and then decreased dramatically in the θ-Al_2O_3 dominated sample to 1.4 and 4.5%. Since no γ-Al_2O_3 is detected by XRD in both the δ-Al_2O_3 and θ-Al_2O_3 dominated samples (Table 1), the $Al_O^{(4)}$ and $Al_T^{(3)}$ sites are then assigned to be associated with the δ-Al_2O_3 phase as these sites are the most prominent in the δ-Al_2O_3 dominated sample. Taking these new assessments in hand where $Al_O^{(1)}$, $Al_O^{(2)}$, $Al_O^{(4)}$, $Al_T^{(2)}$, and $Al_T^{(3)}$ are all related to Al sites in δ-Al_2O_3, the ratio of Al_O/Al_T in the three samples is 1.93, 1.90, and 2.03. These values are closer to an O_h/T_d of 1.66 than of 3, maintaining the previous assessment of δ-Al_2O_3 with vacancies occupying predominantly O_h interstices.

The relative intensity of $Al_O^{(3)}$ and $Al_T^{(1)}$ sites across all samples is almost equal within experimental uncertainty, (1.10, 1.10, and 1.12 for the γ-Al_2O_3, δ-Al_2O_3, and θ-Al_2O_3 samples, respectively, see Table 2). This is evidence that $Al_O^{(3)}$ and $Al_T^{(1)}$ are related to each other. The fact that the relative intensity of these features increases between the γ-Al_2O_3 and δ-Al_2O_3 samples and dramatically increases for the θ-Al_2O_3 sample up to 64% suggests that it is related to the θ-phase, especially considering that the XRD results suggest a 69% θ-Al_2O_3 phase. It is commonly accepted that the structure of the θ-phase is a structural isomorph of β-Ga_2O_3, with the aluminum cations equally distributed over octahedral and tetrahedral sites, giving rise to Al_O/Al_T = 1.0 in an ideal case.[10] This is the approximate ratio between $Al_O^{(3)}$ and $Al_T^{(1)}$. However, recent work has combined NMR and XRD methods to show that the actual fraction of tetrahedral sites in the complex microstructure of θ-Al_2O_3 is ∼42%.[27] Taking into account all sites that may reflect Al species in θ-Al_2O_3 ($Al_O^{(1+3)}$ and $Al_T^{(1)}$), we can arrive at adjusted tetrahedral aluminum fractions proposed for θ-Al_2O_3 in these samples of 39.6, 45.8, and 40.2%, for γ-Al_2O_3, δ-Al_2O_3, and θ-Al_2O_3, respectively. These values match well the more robust description of the site composition of θ-Al_2O_3.

θ-Al_2O_3 is the final transition alumina phase before transformation to the final thermally stable α-Al_2O_3 phase. It is well-known that when transition alumina undergoes the conversion to α-Al_2O_3, significant grain growth occurs,[53] and θ-Al_2O_3 has been reported to transform to α-Al_2O_3 at a nanocrystal size between 10 and 20 nm.[54] Considering the size of our samples, 15 ± 1 and 23 ± 4 nm for the δ-Al_2O_3 and θ-Al_2O_3 dominated samples, respectively, it is reasonable that small domains with local octahedral Al site structure (<1 nm) similar to that of α-Al_2O_3, thus the similar ^{27}Al chemical shifts, may have formed in the θ-Al_2O_3 sample, as suggested by XRD. Such minority species would contribute to the intensity of

https://dx.doi.org/10.1021/acsomega.0c06163
ACS Omega 2021, 6, 4090−4099

Table 3. Spin−Lattice Relaxation Times (T_1) of Each Site in the Three Samples, by Fitting the Intensity of Each Aluminum Site as a Function of Saturation Recovery Time[a]

	sample A (100% γ-Al_2O_3)		sample B (δ-Al_2O_3 dominant)		sample C (θ-Al_2O_3 dominant)	
^{27}Al NMR peak (aluminum sites)	T_{1slow}/s (fraction)	T_{1fast}/s (fraction)	T_{1slow}/s (fraction)	T_{1fast}/s (fraction)	T_{1slow}/s (fraction)	T_{1fast}/s (fraction)
$Al_O^{(1)}$	19.6(79%)	0.8(21%)	15.6(82%)	0.7(18%)	29.9(80%)	0.2(20%)
$Al_O^{(2)}$	7.6(77%)	0.1(23%)	9.7(74%)	0.1(26%)	11.4(83%)	0.1(17%)
$Al_O^{(3)}$	6.1(70%)	0.2(30%)	7.8(89%)	0.05(11%)	13.9(83%)	0.9(17%)
$Al_O^{(4)}$	12.7(77%)	0.3(23%)	10.8(80%)	0.2(20%)	1.2(100%)	
$Al_T^{(1)}$	5.3(79%)	0.1(21%)	7.3(90%)	0.2(10%)	15.7(92%)	0.4(8%)
$Al_T^{(2)}$	11.9(72%)	0.4(28%)	16.6(82%)	0.2(18%)	14.5(79%)	0.2(21%)
$Al_T^{(3)}$	10.3(100%)		16.0(81%)	1.1(19%)	10.0(88%)	0.7(12%)

[a]It is necessary for most of the sites to use a double exponential rise function to fit well with the experiment results. The corresponding T_1 is divided into two parts: T_{1slow} and T_{1fast}, and their fractions are determined.

signals in the octahedral region and may well overlap with signals at $Al_O^{(1)}$.

Based on the above discussions and the assignments of the various octahedral and tetrahedral Al sites in both the δ-Al_2O_3 and θ-Al_2O_3 dominant sample by ^{27}Al MAS NMR spectra, it becomes obvious that the Al sites in the so-called 100% γ-Al_2O_3 sample defined by XRD, in fact, consist of Al site structures with the local electronic environment (including structures with sizes of ∼2 nm or less) similar to the structure units found in both the δ-Al_2O_3 and θ-Al_2O_3 phases (see Table 2 for details). The notable differences are that the structures in γ-Al_2O_3 are less ordered, i.e., more disordered with the least long-range periodicity. Given the fact that there are numerous δ-Al_2O_3 phase structures identified by XRD, so are for the θ-Al_2O_3 phase structures, such complexity combined with the least ordering is most likely the major reason responsible for the relatively broad ^{27}Al peaks in both the octahedral and the tetrahedral Al sites compared to those observed in the δ-Al_2O_3 and θ-Al_2O_3 phases. This may also be the reason why the XRD pattern is also the broadest among the three specially made samples (Figure S1a).

γ-Al_2O_3 is often regarded as a defective spinel structure; however, the true nature of the phase is not yet fully described. δ-Al_2O_3 is said to be composed of two intergrowths ($\delta_{1,2}$ and $\delta_{2,3,4}$), which are composed of the δ_1, δ_2, δ_3, and δ_4 variants. The first two variants contain a slight difference in structure, and the latter three have slightly different translations/rotations. In all, these variants are responsible for 57 unique Al sites.[26] In contrast, θ-Al_2O_3 is composed of an intergrowth of just two variants, β-Ga_2O_3 with motifs of a monoclinic phase related to δ_3-Al_2O_3. As for Al local environments, the amorphous phase cannot be detected by the XRD technique. Thus, 1D and 2D NMR measurement was utilized to provide information of Al local environments. The results are detailed in Table 2. $Al_O^{(4)}$ and $Al_T^{(3)}$ are ascribed to the disordered δ phase. In γ-Al_2O_3, $Al_O^{(1)}$, $Al_O^{(2)}$, $Al_O^{(4)}$, $Al_T^{(2)}$, and $Al_T^{(3)}$ are assigned to local structure similar to the δ phase, and $Al_O^{(3)}$ and $Al_T^{(1)}$ are related with the θ phase. The Al sites in γ-Al_2O_3 are all similar to the sites associated with the θ and δ phase albeit the long-range ordering is different, i.e., crystalline phases have long-range ordering while the amorphous phase has none.

Outlined below, spin−lattice relaxation times (T_1) of the various Al_O and Al_T sites were measured using the standard saturation recovery method. For each spectrum acquired at a specific recovery time (Figure 3a−c), the isotropic chemical shifts and the C_Q values of various Al_O and Al_T sites extracted from 2D experiments in Table 2 are used to fit the 1D spectrum, allowing less than 5% of variation of the parameters during fit optimization. The relative integrated intensity of each site as a function of recovery times is obtained and simulated as illustrated in Figure 3d−f. The relaxation data for most of the Al sites cannot be fit using a single exponential function, so a double-exponential function with distinct relaxation times, i.e., a fast-relaxing component (T_{1fast}) and a slow-relaxing component (T_{1slow}), was employed. The measured relaxation times for the two components and their relative abundance are summarized in Table 3. Due to the restricted freedom of motion in solid-state NMR, increased molecular/segmental motion often means a shorter T_1 value.[55] Thus, the fast-relaxing component is related to increased freedom of motion due to small cluster sizes or aluminum atoms in more disordered/less ordered structures. It can be deduced from the presented fractions that there are more disordered structures in the γ-Al_2O_3 sample and the fewest in the θ-Al_2O_3 samples, supporting the results obtained from the quantitative 1D NMR results discussed above. Furthermore, it is shown that the distorted structures with short relaxation time are selectively enhanced at short recovery times, validating that the fast-relaxing component is, indeed, a more disordering of the structures. For example, the pentahedral part of γ-Al_2O_3 is more apparent at short recovery times with its T_1 = 0.02 s. The broad line peaks of δ-Al_2O_3 acquired at a recovery time of 0.15 s are visually quite similar to the features of γ-Al_2O_3 in both the octahedral and tetrahedral spectral regions. At longer recovery times, the intensity of the slow-relaxing component grows, with the octahedral component of δ-Al_2O_3 split into two peaks ($Al_O^{(2)}$ and $Al_O^{(3)}$). Further, $Al_O^{(3)}$ grows faster than $Al_O^{(2)}$, which is also reflected by their measured relaxation times. As such, it is necessary to wait until the spins are fully relaxed in order to get a quantitative 1D spectrum. The results of the T_1 measurements may indicate the following: (1) Comparison of the spectra of 10 ms, 30 ms, 50 ms, 100 ms, and 1 s of the γ-Al_2O_3 dominated sample (Figure S2) illustrates that for the γ-Al_2O_3 dominated sample, the line shape does not change much with the recovery time; (2) comparison of short recovery time spectra for δ-Al_2O_3 and θ-Al_2O_3 dominated spectra with that of the γ-Al_2O_3 dominated sample clearly shows similar spectral features in terms of both the overall peak line shape and the relaxation time. This again emphasizes that the short relaxing time spectra from both the δ-Al_2O_3 and θ-Al_2O_3 dominated samples contain Al site structures similar to those found in the γ-Al_2O_3 phase, meaning similar local electronic structures. The results further strengthen the concept discussed above that the γ-Al_2O_3 phase (an XRD distinction) is, indeed, a composition of Al

https://dx.doi.org/10.1021/acsomega.0c06163
ACS Omega 2021, 6, 4090−4099

sites with local structures similar to those found in δ-Al_2O_3 and θ-Al_2O_3 phases. Such observations are where NMR can make a significant contribution to understanding the structural properties of transition aluminas and where XRD suffers from challenges impacted by a lack of long-range order.

CONCLUSIONS

High-resolution 1D and 2D ^{27}Al MAS NMR spectra of three alumina samples where the γ-, δ-, or θ-phase was dominantly expressed by controlling the synthesis were obtained at a high field of 850 MHz (19.7 T). Six aluminum sites were resolved in the 2D MQ MAS NMR spectra, and seven aluminum sites are required to fit the quantitative 1D MAS NMR spectra. The spectral assignments as well as the isotropic chemical shift values and the quadrupolar coupling constants related to these sites were subsequently determined. A set of dominant peaks (i.e., $Al_O^{(3)}$ and $Al_T^{(1)}$) with well-defined quadrupolar line shapes was clearly defined in the θ-phase dominant sample and is unambiguously assigned to the θ-Al_2O_3 phase. The combination of the distinct line shapes and peak positions related to the θ-Al_2O_3 phase provided the opportunity for effectively deconvoluting the more complex spectrum obtained from the δ-Al_2O_3 dominant sample, allowing the peaks/quadrupolar parameters related to the δ-Al_2O_3 phase to be extracted with the aid of DMFIT. The results show that the δ-Al_2O_3 phase contains three distinct Al_O sites (i.e., $Al_O^{(1)}$, $Al_O^{(2)}$, and $Al_O^{(4)}$) and two distinct Al_T sites (i.e., $Al_T^{(2)}$ and $Al_T^{(3)}$). This Al site structural information offers a powerful way of analyzing the most complex γ-Al_2O_3 spectrum (100% γ-Al_2O_3 distinction measured by XRD). It is found that the γ-Al_2O_3 phase consists of Al sites with local structures similar to those found in both the δ-Al_2O_3 phase and the θ-Al_2O_3 phase albeit with less ordering (i.e., more distorted). Spin−lattice relaxation time measurement further confirms the disordering of the lattice. For the θ-Al_2O_3 dominated sample, an additional $Al_T^{(4)}$ site (C_Q = 7.3 MHz, η = 0.6) with a fraction of 1.34% is found and is most likely associated with disordered regions near the θ-Al_2O_3 phase structure that has not yet been reported before due to difficulties in observation at lower magnetic fields. Collectively, this study uniquely assigns ^{27}Al features (both octahedral and tetrahedral in nature), which serves to represent the types of Al species present in the θ-Al_2O_3 and δ-Al_2O_3 phases present in transition aluminas, offering a simplified method to quantify complex mixtures of alumina phases and sites in transition alumina samples.

EXPERIMENTAL SECTION

γ-, δ-, and θ-dominant Al_2O_3 samples, herein termed γ-Al_2O_3, δ-Al_2O_3, and θ-Al_2O_3, respectively, were synthesized from aluminum isopropoxide by the hydrolysis method as previously reported.[56] Approximately 10 g of aluminum isopropoxide was added to ∼50 mL of water with vigorous stirring at 80 °C for 1 h. The mixture was subsequently transferred to a 125 mL Teflon liner inside a Parr vessel, which was heated in an oven at 200 °C for 24 h. After cooling to room temperature, the powder was collected by filtration, washed extensively with distilled water, and dried at 100 °C to generate the parent boehmite. The powder of boehmite was then converted to γ-Al_2O_3 by calcination at 800 °C for 2 h, δ-Al_2O_3 by calcination at 1000 °C for 6 h, and θ-Al_2O_3 by calcination at 1100 °C for 3 h.

XRD measurements were carried out on a Philips PW3040/00 X'Pert powder X-ray diffractometer using Cu Kα radiation (λ = 1.5406 Å) in step mode between 2θ values of 15 and 75° with a step size of 0.02°/s. Data analysis was accomplished using Rietveld refinement with crystal structures reported earlier[25−27] using TOPAS v5 (Bruker AXS). Crystallite sizes were estimated from line broadening with instrumental breadths calculated using the fundamental parameter approach.

All ^{27}Al MAS NMR experiments were performed at room temperature on a Varian-Inova 850 MHz NMR spectrometer, operating at a magnetic field of 19.9 T. The corresponding ^{27}Al Larmor frequency was 221.412 MHz. All 1D spectra were acquired at a sample spinning rate of 20 kHz ± 1 Hz, using a commercial 3.2 mm pencil-type MAS probe. A saturation recovery pulse sequence with the saturation segment consisting of a train of hard 90° pulses (50 pulses) with the pulse width of 1.2 μs for each pulse and a pulse spacing of 5 μs was used to obtain spin−lattice relaxation times (T_1), where the recovery time varies between 500 μs and 100 s. Then, during the recovery time, the signal gradually grows back as a function of the recovery time. The number of pulses and the pulse spacing were adjusted to meet the saturation requirement. Each spectrum was acquired using a total of 192 scans with a π/2 read pulse and an acquisition time of 25 ms. The ^{27}Al 3Q MAS NMR spectra at selected recovery times between 0.005 and 30 s were obtained using a z-filter 3Q MAS pulse sequence by inserting the same saturation segment as the 1D at the beginning of the 3Q MAS sequence at a sample spinning rate of 20 kHz ± 1 Hz. The optimized pulse widths were p1 = 2.4 μs, p2 = 0.9 μs, and p3 = 10.0 μs. In the hypercomplex 3Q MAS experiment, 96 transients for either the real and imaginary F1 FID were collected for each of the 90−192 evolution increments for the three samples. The acquisition time was 10 ms. Spectral widths for the F2 (acquisition) and F1 (evolution) dimensions were 100 and 40 kHz, respectively. All spectra were externally referenced to a 1 M $Al(NO_3)_3$ aqueous solution at 0 ppm. DMFIT was the software package used to simulate the spectra and fit the peaks.[57]

ASSOCIATED CONTENT

Supporting Information

The Supporting Information is available free of charge at https://pubs.acs.org/doi/10.1021/acsomega.0c06163.

XRD patterns of transition aluminas and spin−lattice relaxation NMR spectra (PDF)

AUTHOR INFORMATION

Corresponding Authors

Yong Wang − *Institute for Integrated Catalysis and Environmental Molecular Sciences Laboratory, Pacific Northwest National Laboratory, Richland, Washington 99354, United States; Gene and Linda Voiland School of Chemical Engineering, Washington State University, Pullman, Washington 90015, United States;* orcid.org/0000-0002-8460-7410; Email: Yong.Wang@pnnl.gov

Jian Zhi Hu − *Institute for Integrated Catalysis and Environmental Molecular Sciences Laboratory, Pacific Northwest National Laboratory, Richland, Washington 99354, United States;* orcid.org/0000-0001-8879-747X; Email: Jianzhi.Hu@pnnl.gov

https://dx.doi.org/10.1021/acsomega.0c06163
ACS Omega 2021, 6, 4090−4099

Authors

Suochang Xu − *Institute for Integrated Catalysis and Environmental Molecular Sciences Laboratory, Pacific Northwest National Laboratory, Richland, Washington 99354, United States; Dalian Institute of Chemical Physics, the Chinese Academy of Sciences, Dalian 116023, P.R. China*

Nicholas R. Jaegers − *Institute for Integrated Catalysis and Environmental Molecular Sciences Laboratory, Pacific Northwest National Laboratory, Richland, Washington 99354, United States; Gene and Linda Voiland School of Chemical Engineering, Washington State University, Pullman, Washington 90015, United States;* orcid.org/0000-0002-9930-7672

Wenda Hu − *Institute for Integrated Catalysis and Environmental Molecular Sciences Laboratory, Pacific Northwest National Laboratory, Richland, Washington 99354, United States; Gene and Linda Voiland School of Chemical Engineering, Washington State University, Pullman, Washington 90015, United States*

Ja Hun Kwak − *Institute for Integrated Catalysis and Environmental Molecular Sciences Laboratory, Pacific Northwest National Laboratory, Richland, Washington 99354, United States; Ulsan National Institute of Science and Technology (UNIST), Ulsan 689-798, Korea;* orcid.org/0000-0001-5245-0765

Xinhe Bao − *Dalian Institute of Chemical Physics, the Chinese Academy of Sciences, Dalian 116023, P.R. China;* orcid.org/0000-0001-9404-6429

Junming Sun − *Gene and Linda Voiland School of Chemical Engineering, Washington State University, Pullman, Washington 90015, United States;* orcid.org/0000-0002-0071-9635

Complete contact information is available at: https://pubs.acs.org/10.1021/acsomega.0c06163

Notes

The authors declare no competing financial interest.

■ ACKNOWLEDGMENTS

The research at PNNL was supported by the U.S. Department of Energy, Office of Science, Office of Basic Energy Sciences, Division of Chemical Sciences, Geosciences, and Biosciences. Experiments were conducted in the Environmental Molecular Sciences Laboratory (grid.436923.9), a DOE Office of Science User Facility located at the Pacific Northwest National Laboratory (PNNL). PNNL is a multiprogram national laboratory operated by Battelle for the U.S. Department of Energy under contract DE-AC05-76RL01830. J.H.K. was supported by the Basic Science Research Program through the National Research Foundation of Korea (NRF) funded by the Ministry of Education, Science and Technology (2.120238.01). The authors wish to acknowledge Mark Bowden and Libor Kovark for their assistance with XRD experiments, their insights into the XRD results, and their thorough discussions on transition aluminas. The authors also wish to acknowledge Mary Y. Hu, Amity Andersen, Chares H. F. Peden, János Szanyi, and Xiuwen Han for their useful discussions.

■ REFERENCES

(1) Ipatiew, W. Zur Frage Über die Zersetzung des Äthylalkohols in Gegenwart verschiedener Katalysatoren. *J. Prakt. Chem.* **1903**, *67*, 420−422.

(2) Konstantin, K.; Nicholas, R. J.; Ja-Hun, K.; János, S.; Libor, K. *Precise Identification and Characterization of Catalytically Active Sites on the Surface of γ-Alumina*; *ChemRxiv* 2020.

(3) Wan, C.; Hu, M. Y.; Jaegers, N. R.; Shi, D.; Wang, H.; Gao, F.; Qin, Z.; Wang, Y.; Hu, J. Z. Investigating the Surface Structure of Gammaγ- Al_2O_3 Supported Wo_x Catalysts by High Field ^{27}Al-27 Mas NMR and Electronic Structure Calculations. *J. Phys. Chem. C* **2016**, *120*, 23093−23103.

(4) Kumari, U.; Behera, S. K.; Meikap, B. C. A Novel Acid Modified Alumina Adsorbent with Enhanced Defluoridation Property: Kinetics, Isotherm Study and Applicability on Industrial Wastewater. *J. Hazard. Mater.* **2019**, *365*, 868−882.

(5) Schmidt, A.; Salomon, A.; Dudczig, S.; Berek, H.; Rafaja, D.; Aneziris, C. G. Functionalized Carbon-Bonded Filters with an Open Porous Alumina Coating: Impact of Time on Interactions and Steel Cleanliness. *Adv. Eng. Mater.* **2017**, *19*, 1700170.

(6) Godino, L.; Pombo, I.; Girardot, J.; Sanchez, J. A.; Iordanoff, I. Modelling the Wear Evolution of a Single Alumina Abrasive Grain: Analyzing the Influence of Crystalline Structure. *J. Mater. Process. Technol.* **2020**, *277*, 116464.

(7) Hubadillah, S. K.; Othman, M. H. D.; Ismail, A. F.; Rahman, M. A.; Jaafar, J.; Iwamoto, Y.; Honda, S.; Dzahir, M. I. H. M.; Yusop, M. Z. M. Fabrication of Low Cost, Green Silica Based Ceramic Hollow Fibre Membrane Prepared from Waste Rice Husk for Water Filtration Application. *Ceram. Int.* **2018**, *44*, 10498−10509.

(8) Hudson, L. K.; Misra, C.; Perrotta, A. J.; Wefers, K.; Williams, F. S. Aluminum Oxide. In *Ullmann's Encyclopedia of Industrial Chemistry*; Wiley-VCH Verlag GmbH & Co. KGaA: 2000.

(9) Jayaram, V.; Levi, C. G. The Structure of δ-Alumina Evolved from the Melt and the γ → δ Transformation. *Acta Metall. Mater.* **1989**, *37*, 569−578.

(10) Levin, I.; Brandon, D. Metastable Alumina Polymorphs: Crystal Structures and Transition Sequences. *J. Am. Ceram. Soc.* **1998**, *81*, 1995−2012.

(11) McHale, J. M. Surface Energies and Thermodynamic Phase Stability in Nanocrystalline Aluminas. *Science* **1997**, *277*, 788−791.

(12) Schaper, H.; Doesburg, E. B. M.; Van Reijen, L. L. The Influence of Lanthanum Oxide on the Thermal-Stability of γ Alumina Catalyst Supports. *Appl. Catal.* **1983**, *7*, 211−220.

(13) Kwak, J. H.; Hu, J.; Lukaski, A.; Kim, D. H.; Szanyi, J.; Peden, C. H. F. Role of Pentacoordinated Al^{3+} Ions in the High Temperature Phase Transformation of γ - Al_2O_3. *J. Phys. Chem. C* **2008**, *112*, 9486−9492.

(14) Wang, Q.; Li, W.; Hung, I.; Mentink-Vigier, F.; Wang, X.; Qi, G.; Wang, X.; Gan, Z.; Xu, J.; Deng, F. Mapping the Oxygen Structure of γ- Al_2O_3 by High-Field Solid-State Nmr Spectroscopy. *Nat. Commun.* **2020**, *11*, 3620.

(15) Li, W.; Wang, Q.; Xu, J.; Aussenac, F.; Qi, G.; Zhao, X.; Gao, P.; Wang, C.; Deng, F. Probing the Surface of γ- Al_2O_3 by Oxygen-17 Dynamic Nuclear Polarization Enhanced Solid-State NMR Spectroscopy. *Phys. Chem. Chem. Phys.* **2018**, *20*, 17218−17225.

(16) Lee, J.; Jeon, H.; Oh, D. G.; Szanyi, J.; Kwak, J. H. Morphology-Dependent Phase Transformation of γ- Al_2O_3. *Appl. Catal. A: Gen.* **2015**, *500*, 58−68.

(17) Zhou, R.-S.; Snyder, R. L. Structures and Transformation Mechanisms of the η, γ and Θ Transition Aluminas. *Acta Cryst.* **1991**, *47*, 617−630.

(18) Paglia, G.; Buckley, C. E.; Udovic, T. J.; Rohl, A. L.; Jones, F.; Maitland, C. F.; Connolly, J. Boehmite-Derived γ-Alumina System. 2. Consideration of Hydrogen and Surface Effects. *Chem. Mater.* **2004**, *16*, 1914−1923.

(19) Wolverton, C.; Hass, K. C. Phase Stability and Structure of Spinel-Based Transition Aluminas. *Phys. Rev. B* **2000**, *63*, No. 024102.

(20) Paglia, G.; Buckley, C. E.; Rohl, A. L.; Hunter, B. A.; Hart, R. D.; Hanna, J. V.; Byrne, L. T. Tetragonal Structure Model for Boehmite-Derived γ-Alumina. *Phys. Rev. B* **2003**, *68*, 144110.

(21) Digne, M.; Sautet, P.; Raybaud, P.; Euzen, P.; Toulhoat, H. Use of Dft to Achieve a Rational Understanding of Acid-Basic Properties of γ-Alumina Surfaces. *J. Catal.* **2004**, *226*, 54−68.

(22) Paglia, G. Ph.D. Thesis. Curtin University of Technology; 2004.
(23) Paglia, G.; Rohl, A. L.; Buckley, C. E.; Gale, J. D. Determination of the structure of γ-alumina from interatomic potential and first-principles calculations: The requirement of significant numbers of nonspinel positions to achieve an accurate structural model. *Phys. Rev. B* **2005**, *71*, 224115.
(24) Wefers, K.; Misra, C. *Oxides and Hydroxides of Aluminium: Alcoa Technical Paper No. 19*; Alcoa Laboratories: Pittsburgh, 1987.
(25) Kovarik, L.; Bowden, M.; Genc, A.; Szanyi, J.; Peden, C. H. F.; Kwak, J. H. Structure of δ-Alumina: Toward the Atomic Level Understanding of Transition Alumina Phases. *J. Phys. Chem. C* **2014**, *118*, 18051−18058.
(26) Kovarik, L.; Bowden, M.; Shi, D.; Szanyi, J.; Peden, C. H. F. Structural Intergrowth in δ - Al_2O_3. *J. Phys. Chem. C* **2019**, *123*, 9454−9460.
(27) Kovarik, L.; Bowden, M.; Shi, D.; Washton, N. M.; Andersen, A.; Hu, J. Z.; Lee, J.; Szanyi, J.; Kwak, J. H.; Peden, C. H. F. Unraveling the Origin of Structural Disorder in High Temperature Transition Al_2O_3: Structure of Θ-Al2o3. *Chem. Mater.* **2015**, *27*, 7042−7049.
(28) Kovarik, L.; Bowden, M.; Andersen, A.; Jaegers, N. R.; Washton, N.; Szanyi, J. Quantification of High-Temperature Transition $Al_2o_3$and Their Phase Transformations**. *Angew. Chem., Int. Ed.* **2020**, *59*, 21719−21727.
(29) Weibel, A.; Bouchet, R.; Boulc', F.; Knauth, P. The Big Problem of Small Particles: A Comparison of Methods for Determination of Particle Size in Nanocrystalline Anatase Powders. *Chem. Mater.* **2005**, *17*, 2378−2385.
(30) O'Connell, K.; Regalbuto, J. R. High Sensitivity Silicon Slit Detectors for 1 nm Powder Xrd Size Detection Limit. *Catal. Lett.* **2015**, *145*, 777−783.
(31) Chauhan, A.; Chauhan, P. Powder Xrd Technique and Its Applications in Science and Technology. *J. Anal. Bioanal. Tech.* **2014**, *5*, 1−5.
(32) Pecharromán, C.; Sobrados, I.; Iglesias, J. E.; González-Carreño, T.; Sanz, J. Thermal Evolution of Transitional Aluminas Followed by Nmr and Ir Spectroscopies. *J Phys Chem B* **1999**, *103*, 6160−6170.
(33) Das, R. N.; Hattori, A.; Okada, K. Influence of Processing Medium on Retention of Specific Surface Area of γ-Alumina at Elevated Temperature. *Appl. Catal., A* **2001**, *207*, 95−102.
(34) O'Dell, L. A.; Savin, S. L. P.; Chadwick, A. V.; Smith, M. E. A Al^{-27} Mas Nmr Study of a Sol-Gel Produced Alumina: Identification of the Nmr Parameters of the θ-Al_2o_3 Transition Alumina Phase. *Solid State Nucl. Magn. Reson.* **2007**, *31*, 169−173.
(35) Huggins, B. A.; Ellis, P. D. Aluminum-27 Nuclear Magnetic Resonance Study of Aluminas and Their Surfaces. *J. Am. Chem. Soc.* **1992**, *114*, 2098−2108.
(36) Coster, D.; Blumenfeld, A. L.; Fripiat, J. J. Lewis Acid Sites and Surface Aluminum in Aluminas and Zeolites: A High-Resolution Nmr Study. *J. Phys. Chem.* **1994**, *98*, 6201−6211.
(37) Chen, F. R.; Davis, J. G.; Fripiat, J. J. Aluminum Coordination and Lewis Acidity in Transition Aluminas. *J. Catal.* **1992**, *133*, 263−278.
(38) Chandran, C. V.; Kirschhock, C. E. A.; Radhakrishnan, S.; Taulelle, F.; Martens, J. A.; Breynaert, E. Alumina: Discriminative Analysis Using 3d Correlation of Solid-State Nmr Parameters. *Chem. Soc. Rev.* **2019**, *48*, 134−156.
(39) Schmidt-Rohr, K.; Spiess, H. W. *Multidimensional Solid-State Nmr and Polymers*; Academic Press Limited: London 1994.
(40) Smith, S. J.; Amin, S.; Woodfield, B. F.; Boerio-Goates, J.; Campbell, B. J. Phase Progression of γ- Al_2O_3 Nanoparticles Synthesized in a Solvent-Deficient Environment. *Inorg. Chem.* **2013**, *52*, 4411−4423.
(41) Hu, J. Z.; Wan, C.; Vjunov, A.; Wang, M.; Zhao, Z.; Hu, M. Y.; Camaioni, D. M.; Lercher, J. A. 27al Mas Nmr Studies of Hbea Zeolite at Low to High Magnetic Fields. *J. Phys. Chem. C* **2017**, *121*, 12849−12854.
(42) Kwak, J. H.; Hu, J.; Mei, D.; Yi, C.-W.; Kim, D. H.; Peden, C. H. F.; Allard, L. F.; Szanyi, J. Coordinatively Unsaturated Al^{3+} Centers as Binding Sites for Active Catalyst Phases of Platinum on γ-Al_2O_3. *Science* **2009**, *325*, 1670−1673.
(43) Frydman, L.; Harwood, J. S. Isotropic Spectra of Half-Integer Quadrupolar Spins from Bidimensional Magic-Angle-Spinning Nmr. *J. Am. Chem. Soc.* **1995**, *117*, 5367−5368.
(44) Medek, A.; Harwood, J. S.; Frydman, L. Multiple-Quantum Magic-Angle Spinning Nmr: A New Method for the Study of Quadrupolar Nuclei in Solids. *J. Am. Chem. Soc.* **1995**, *117*, 12779−12787.
(45) Rocha, J. Single- and Triple-Quantum ^{27}Al Mas Nmr Study of the Thermal Transformation of Kaolinite. *J. Phys. Chem. B* **1999**, *103*, 9801−9804.
(46) van Bokhoven, J. A.; Roest, A. L.; Koningsberger, D. C.; Miller, J. T.; Nachtegaal, G. H.; Kentgens, A. P. M. Changes in Structural and Electronic Properties of the Zeolite Framework Induced by Extraframework Al and La in H-Usy and La(X)Nay: A ^{29}Si- and ^{27}Al- Mas Nmr and ^{27}Al- Mq Mas Nmr Study. *J. Phys. Chem. B* **2000**, *104*, 6743−6754.
(47) Kentgens, A. P. M.; Iuga, D.; Kalwei, M.; Koller, H. Direct Observation of BrØnsted Acidic Sites in Dehydrated Zeolite H-Zsm5 Using Dfs-Enhanced ^{27}Al- Mqmas Nmr Spectroscopy. *J. Am. Chem. Soc.* **2001**, *123*, 2925−2926.
(48) Wang, Y. G.; Bronsveld, P. M.; DeHosson, J. T. M.; Djuričić, B.; McGarry, D.; Pickering, S. Ordering of Octahedral Vacancies in Transition Aluminas. *J. Am. Ceram. Soc.* **1998**, *81*, 1655−1660.
(49) Hill, M. R.; Bastow, T. J.; Celotto, S.; Hill, A. J. Integrated Study of the Calcination Cycle from Gibbsite to Corundum. *Chem. Mater.* **2007**, *19*, 2877−2883.
(50) Hu, J. Z.; et al. High Field 27al Mas Nmr and Tpd Studies of Active Sites in Ethanol Dehydration Using Thermally Treated Transitional Aluminas as Catalysts. *J. Catal.* **2016**, *336*, 85−93.
(51) Wilson, S. J. The Dehydration of Boehmite, γ-Alooh, to γ-Al_2O_3. *J. Solid State Chem.* **1979**, *30*, 247−255.
(52) Wilson, S. J.; Mc Connell, J. D. C. A kinetic study of the system γ-AlOOHAl2O3. *J. Solid State Chem.* **1980**, *34*, 315−322.
(53) Legros, C.; Carry, C.; Bowen, P.; Hofmann, H. Sintering of a Transition Alumina: Effects of Phase Transformation, Powder Characteristics and Thermal Cycle. *Int. J. High Technol. Ceram.* **1999**, *19*, 1967−1978.
(54) Mo, S. D.; Ching, W. Y. Electronic and Optical Properties of θ-Al_2O_3 and Comparison to α- Al_2O_3. *Phys. Rev. B* **1998**, *57*, 15219−15228.
(55) Slichter, C. P. *Principles of Magnetic Resonance*; Springer Berlin Heidelberg: New York, 1990.
(56) Kovarik, L.; Genc, A.; Wang, C.; Qiu, A.; Peden, C. H. F.; Szanyi, J.; Kwak, J.-H. Tomography and High-Resolution Electron Microscopy Study of Surfaces and Porosity in a Plate-Like γ-Al_2O_3. *J. Phys. Chem. C* **2013**, *117*, 179−186.
(57) Massiot, D.; Fayon, F.; Capron, M.; King, I.; Le Calvé, S.; Alonso, B.; Durand, J.-O.; Bujoli, B.; Gan, Z.; Hoatson, G. Modelling One- and Two-Dimensional Solid-State Nmr Spectra. *Magn. Reson. Chem.* **2002**, *40*, 70−76.

https://dx.doi.org/10.1021/acsomega.0c06163
ACS Omega 2021, 6, 4090−4099